GEO India 2018

PaperID **AU291**

Author **Ashish Misra , ONGC , India**

Co-Authors **B.K. Mishra, Blecy Tep, Simantini Pattanayak**

Thermal Remote Sensing for Regional Lithological in-fill Mapping in a Densely Vegetated Terrain: Case of Andaman Islands

Ashish Misra*, B.K. Mishra, Blecy Tep & Simantini Pattanayak
Remote Sensing & Geomatics, Geology Group, KDMIPE, ONGC
*Corresponding author, email: misra_ashish@ongc.co.in

Abstract

Vast areas in Middle and South Andaman Islands covered by thick tropical vegetation and reserved for the native Jarawa tribals continue to remain geologically unmapped through field-based direct investigations. These mapping gaps have been chosen as test areas to evaluate the potential of advanced remote sensing techniques to provide an alternative means of extending field knowledge from adjacent mapped areas to these data gaps. In view of the limitations of conventional optical remote sensing in penetrating the thick vegetation overgrowth concealing the outgrop lithology, thermal remote sensing radiance and emissivity data in the wavelength range of 8-12 μm have been utilized. Despite known adverse influence of vegetal presence in spectral response of bare rock/ soil surface even in the thermal infrared range, the digitally enhanced thermal radiance data, along with spectral indices related to dominant mineralogical sub-categories expected in the terrain, *viz*. quartz-rich, mafic-rich and carbonate-rich rock types, have yielded interesting spectral responses. These results are meaningfully correlated with the outcrop lithologies mapped through field investigations, and can therefore be extended to the unmapped areas with a high degree of confidence, by analogy. Quantitative remote sensing techniques of full spectral classification, and estimation of silica weight percentages as an indirect measure of corresponding lithological category, have further affirmed the utility of remote sensing technology as a viable tool to supplement field mapping efforts in logistically difficult and inaccessible areas.

A. Introduction

Surface geological mapping is fundamental to exploration of natural resources, including hydrocarbons. Exploratory confidence in subsurface investigations requires high quality surface correlations. In tectonically complex accretionary prism setup like that of Andaman-Nicobar Island arc, the need for detailed surface geological mapping cannot be overemphasized. Despite this, vast areas in Middle and South Andaman Islands mostly occurring towards west of the prominent east-dipping and west-verging Jarawa Thrust Zone, and covered by thick tropical vegetation and inhabited by the tribal Jarawa community have remained geologically unmapped through field investigations (Figure 1) owing to multiple reasons – hostility of the tribals, remoteness, accessibility limitations, and most importantly – an impenetrably thick vegetation cover.

Attempts to map the terrain utilizing conventional remote sensing (aerial photographs and satellite imagery in visible EMR range) could only yield limited success. Airborne and satellite radar imaging could only succeed in unravelling structural detail further. However, the questions regarding lithological nature of the outcrops concealed by the vegetation have been offered speculative answers based on photogeological interpretations thus far (Prasad et al., 1991; Dotiwala et al., 1998). In this paper, we report the use of thermal infrared remote sensing to offer a more data-driven answer to the above question.

B. Thermal Infrared Spectroscopy of Rocks & Applied Remote Sensing

Most of the important rock-forming silicate minerals have their diagnostic spectral features in the TIR region (7.0-14.0 μm) (Salisbury and D'Aria, 1992). The variation in silicate mineralogy from felsic to mafic is represented as a shift of the main spectral feature (Si-O stretching region or reststrahlen band, Figure 2a-e; Hook et al., 1999) towards longer wavelengths. Another spectral feature in silicate mineral spectra between 8.5 and 12.0 μm occurs due to the H-O-Al bond at 11.0 μm, and is characteristic of

clay minerals. A strong emissivity minimum for carbonates near 11.3 µm (Figure 2f) makes TIR data suitable for mapping of these rock units.

The presence of diagnostic spectral features (reststrahlen band or minima in emissivity curves) of rock forming silicates, sulfates and carbonates in the thermal infrared range (7-15 µm) allows their detection, identification and mapping using remote sensing techniques. Also, the property of a systematic shift in the spectral signatures of silicate minerals, based on their crystal structure (Figure 3) has been used to estimate their absolute quantitative distribution using thermal infrared remote sensing data (Watanabe, 2002; Misra, 2008). All of the above characteristics have been utilized in mapping silicate mineralogy using multi/hyperspectral TIR data (Misra, 2008; van der Meer et al., 2012; Kruse, 2015; Black et al., 2016).

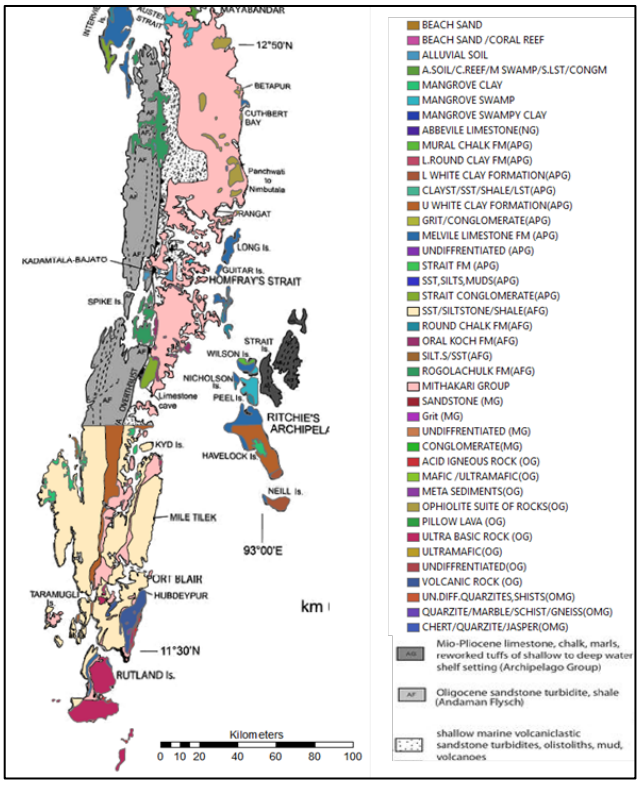

Figure-1: Major data gaps in geological mapping in northwest areas of South Andaman and western parts of Middle Andaman. Map compiled in GIS using GSI Quadrangle Geological maps and Bandhopadhyay & Carter (2017).

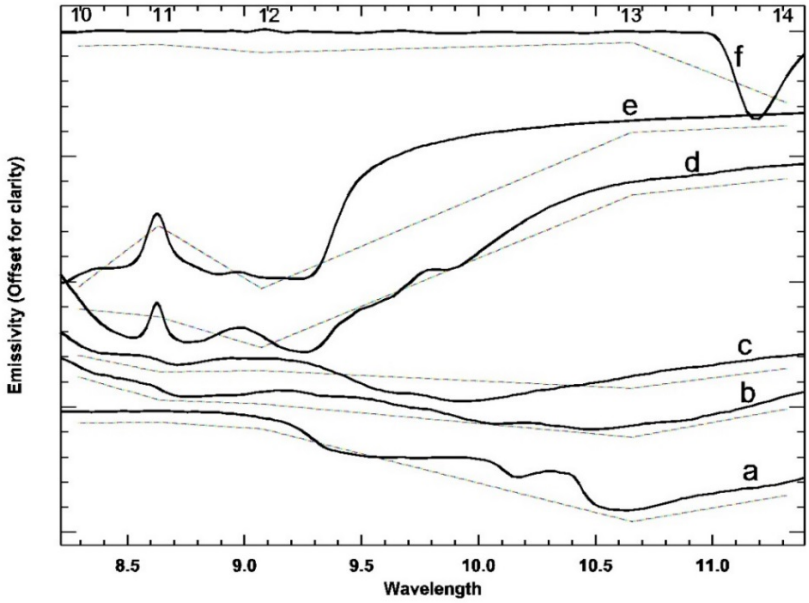

Figure-2: Emissivity spectra of (a) dunite, (b) gabbro, (c) diorite, (d) granite, (e) quartzite, (f) dolomitic marble. Biconical reflectance spectra from JHU spectral library have been converted to emissivity using Kirchhoff's law. The corresponding spectra resampled to ASTER TIR bandpasses have been shown in dashed lines, and the positions of the bands have been marked on the top. Wavelength is in μm. (after Misra, 2008)

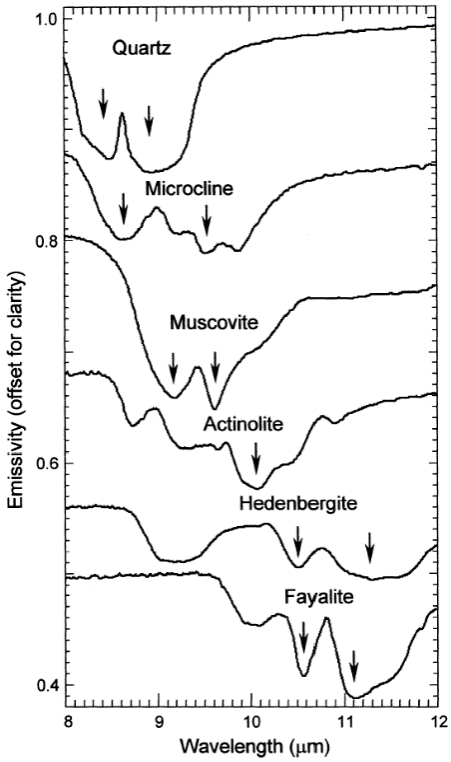

Figure-3: Examples of silicate mineral spectra with emissivity features in the TIR. Spectral features are related to Si-O stretching vibrations within the silicate crystal structure and shift to longer wavelengths with increasing isolation of the SiO_4 tetrahedra. Spectra are from Arizona State University (ASU) thermal emission spectral library.

C. Data & Methodology

Since the region represents diverse silicate mineralogy – from pure felsic rocks to ultramafic rocks, in addition to impure carbonates and abundant clays, it is expected that the spectral contrast among these lithological classes will be useful in detecting their presence and mapping their spatial distribution with the help of thermal infrared remote sensing data. A number of studies using airborne hyperspectral imaging spectroradiometer thermal infrared (TIR) data (such as TIMS, SEBASS, DAIS, IRIS, TASI etc.)

have amply demonstrated the utility of TIR emissivity data in remote lithologic mapping and quantitative mineralogic estimation (Kahle & Goetz, 1983; Vaughan et al., 2003 & 2005; Michalski et al. 2004; Black et al., 2016). However, data from these sensor systems are not available for all areas of the world, while data from the popular Landsat TM/ETM+ sensor have only one broad band in the TIR region (band 6), which cannot be used for detailed mapping of individual silicate mineral species and their abundances. The Advanced Spaceborne Thermal Emission and Reflection radiometer (ASTER) records data in 5 TIR bands in addition to 3 visible-, near-infrared (VNIR) and 6 shortwave-infrared (SWIR) bands (Abrams, 2000). ASTER data are free and available worldwide with different levels of calibration and processing.

In our study, we use cloudfree ASTER level 1B (L1B) radiance-at-sensor, and level 2 (L2) TIR surface radiance and surface emissivity data procured through NASA's earthdata portal (*earthdata.nasa.gov*) to map surface lithology and estimate silica abundance for the thickly vegetated Andaman Islands in the Bay of Bengal.

D. Data Processing

1. Decorrelation Stretch of ASTER L1B TIR Data

The high band-to-band correlation among the TIR radiance-at-sensor data have been removed digitally by applying Decorrelation Stretch (DCS) to a three band composite ASTER TIR bands. DCS suppresses surface temperature effects which dominate the radiant spectral flux measured in all bands, and at the same time enhances subtle spectral features arising from emissivity variations. In DCS, data from three or more bands are transformed to principal components and then stretched to equalize the variance along three statistically independent axes. The stretched data are then transformed back into the approximate original RGB coordinate system for display as a color composite image (Gillespie, 1992). The 'standard' DCS channels are selected such that wavelength channels centered about 10.5 µm (ASTER band 13), 9.2 µm (ASTER band 12), and 8.3 µm (ASTER band 10) are assigned to R-G-B, respectively.

2. Lithological Indices

The indices proposed by Ninomiya et al. (2005) for the ASTER TIR data have been generated using the ASTER L2 TIR surface radiance data for the study area. The various indices are Carbonate Index (CI), Quartz Index (QI), and Mafic Index (MI, and are reproduced below:

Carbonate Index: $CI = \frac{AST\_B13}{AST\_B14}$,

Quartz Index: $QI = \frac{(AST\_B11)^2}{AST\_B10 * AST\_B12}$, and

Mafic Index: $MI = \frac{AST\_B12 * (AST\_B13)^2}{(AST\_B11)^3}$

AST_Bn (where, 10 ≤ n ≤ 14) stands for the ASTER band n.

3. Quantitative Silica Weight Percent Estimation

The silica content image is generated using a revised model of MMAJ's original K-value method (MMAJ, 2001, Watanabe, 2002) and applying it on the ASTER L2 TIR surface emissivity data generated by applying the Temperature and Emissivity Separation (TES) algorithm (Gillespie et al., 1998) to the corresponding L1B TIR data.

The K-value was originally derived using an empirical approach based on laboratory work on 194 samples including both fresh and weathered rocks, and minerals. The revised model defines following simple linear relationship between the empirical K-value and the actual SiO_2 weight per cent:

$$\text{Silica Index} = \frac{B13}{B10}$$

The K-value in the above expression is defined as:

$$K = -\log\left\{\frac{\left(\frac{E10+E11+E12}{3}\right)}{E13}\right\}$$

Where, E*n* is the emissivity for ASTER band *n*.

E. Results, Discussion & Conclusions

The DCS composite of TIR bands 13-12-10 is shown in Figure-4a and the lithological indices are shown in Figure 4b-d. The corresponding silica weight percent image is shown in Figure 4e. On the DCS images, the more siliceous surfaces appear in reds and pinks, such as the arenaceous-argillaceous units of Andaman Flysch and Port Blair/ Archipelago groups. Mafic rocks and clay-rich surfaces appear in blue-violet and magenta-purple hues, respectively. Areas in shades of green are most likely to be mixtures of arable soil/regolith rich in iron, and vegetation (forests and cropland). The intermediate hues represent mixtures of these surfaces. The inherent horizontal banding in the TIR data due to scan-line mismatch can be seen more pronouncedly in the DCS images.

In the lithological indices, it can be readily observed that while there is a general agreement between the mafic index and the expected rock types, the carbonate index is difficult to interpret due to heavy striping noise. Also the quartz and carbonate indices, show overlapping abundances with the mafic index. This can be explained if we look at the emissivity spectrum of mafic carbonate rocks (dolomitic marble; Figure 2f). The spectrum is representative of calcite and dolomite, the two principal carbonate minerals. The emissivity low for carbonates lies close to the emissivity low for the ultramafic rocks (*e.g.*, dunite, Figure 2a). For coarse spectral resolution data as in ASTER TIR, the emissivity minima for carbonates and mafic/ultramafic rocks almost coincide. In addition to this, in the study area, the rocks are rarely pure; they are mafic-rich and are interbedded with ultramafics. While the banding observed in the Carbonate Index image is the result of high correlation between bands 13 and 14.

In the silica weight percent image, greens and yellows typically correspond to siliceous regions, whereas oranges and reds correspond to more mafic surface lithologies. While there is evidently an overestimation of the silica weight percentages for a few ‘dark’ pixels confined to areas with thick canopies and deep hill shadows, over 99.91% of the data is represented by SiO_2 weight percent range of 52.2% to 100%. A corresponding silica index based on band ratio of ASTER L2 surface radiance data (AST_13/AST_10) has also been computed for reference (Figure 4f).

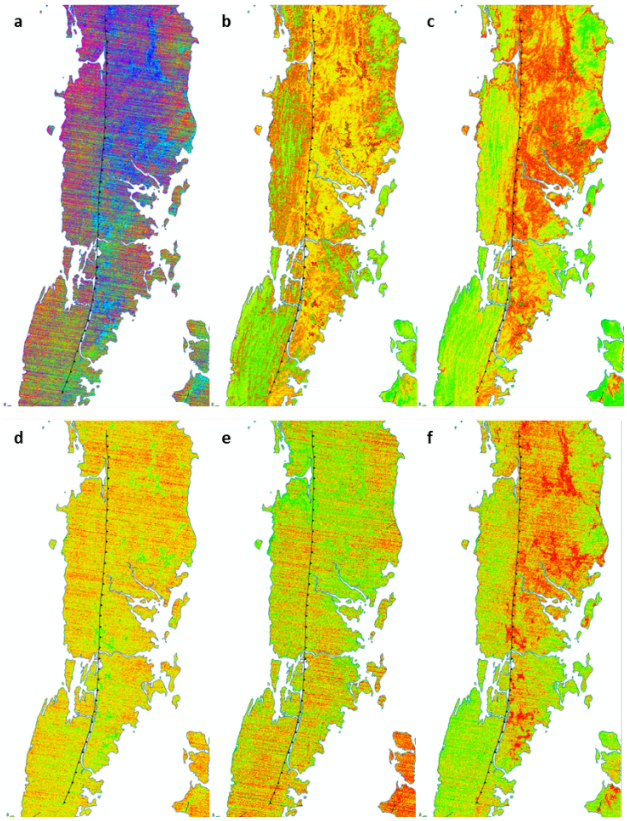

Figure-4: a) Decorrelation Stretch of ASTER bands 13-12-10 in RGB; TIR surface radiance-based lithologic indices for mafic rocks (b), quartz-rich rocks (c) and carbonate rocks (d); silica weight percent map based on ASTER L2 TIR surface emissivity data (e); and ASTER band ratio image for silica abundance (f). In figures b-f green indicates higher abundances for respective lithologic categories. The N-S trending Jarawa Thrust Zone is marked in black.

Combined utility of spectral indices based on TIR surface radiance data and RGB composite of DCS image generated using band combination of 13-12-10 was analysed to extend the mapped units based on their spectral similarity in gap areas. Based on extension of spectral similarity, and integrating quantitative silica weight percent map, the in-fill mapped geological map covering the gap areas was generated as presented in Figure 5. Coarse spatial resolution of the ASTER TIR data (90m) and unresolvable interference of thick vegetation canopy of the gap areas limits more detailed lithological characterization.

The study establishes the potential of thermal remote sensing in mapping lithology in a densely vegetation terrain. With easy availability of spectrally and spatially higher resolution TIR data from a spaceborne platform, better results can be expected in future.

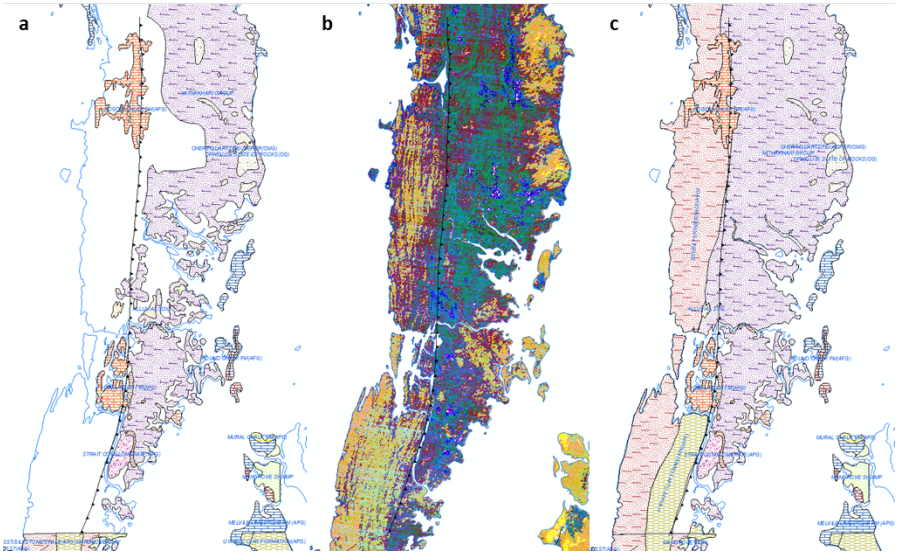

Figure-5: Extending spectral classes in areas of data gaps (a) on the basis of spectral similarity as shown in (c), utilizing spectral indices (colour composite of quartz index (red), mafic index (green) and carbonate index (blue) in (b)) and DCS of TIR surface radiance data and results of quantitative silica weight percent estimation.

References

Abrams, M., (2000). The Advanced Spaceborne Thermal Emission and Reflection Radiometer (ASTER): data products for the high spatial resolution imager on NASA's Terra platform. International Journal of Remote Sensing, vol. 21, pp. 847-859.

Bandopadhyay, P. C. and Carter, A. (eds.) 2017. The Andaman–Nicobar Accretionary Ridge: Geology, Tectonics and Hazards. Geological Society, London, Memoirs, 47.

Black, M., Riley, T.R., Ferrier, G., Fleming, A.H., Fretwell, P.T., (2016) Automated lithological mapping using airborne hyperspectral thermal infrared data: A case study from Anchorage Island, Antarctica, Remote Sensing of Environment, vol. 176, pp. 225-241.

Dotiwala, S., Dotiwala, F., Mitra, D.S., Dey, B.K. (1998) Detailed Structural Mapping of the Exposed Geology of Middle & South Andaman Islands Using High Resolution Visible and Microwave Data, Unpublished ONGC Report

Gillespie, A. R., (1992). Enhancements of multispectral thermal infrared images: de-correlation contrast stretching. Remote Sensing of Environment, 42, pp. 147-156.

Gillespie, A. R., Rokugawa, S., Matsunaga, T., Steven Cothern, J., Hook, S. and Kahle, A. B., (1998). A temperature and emissivity separation algorithm for advanced spaceborne thermal emission and reflection radiometer (ASTER) images. IEEE Transactions on Geoscience and Remote Sensing, 36(4), pp. 1113–1126.

Hook, S. J, Abbott, E. A., Grove, C., Kahle, A. B. and Palluconi, F., (1999). Use of multispectral thermal infrared data in geological studies. In: Rencz AN (ed) Remote Sensing for the Earth Sciences, Manual of Remote Sensing, 3rd edn, vol 3, American Society of Photogrammetry and Remote Sensing, John Wiley, pp 59–110.

Kahle, A. B. and Goetz, A. F. H., (1983). Mineralogic information from a new airborne thermal infra-red multispectral scanner. Science, 222, pp. 24-27.

Kruse, F.A. (2015) Integrated visible and near-infrared, shortwave infrared, and longwave infrared full-range hyperspectral data analysis for geologic mapping. Journ. of Applied Remote Sensing, Vol. 9, 2015, 20 p.

Michalski, J. R., Reynolds, S. J., Sharp, T. G. and Christensen, P. R., (2004). Thermal infrared analysis of weathered granitic rock compositions in the Sacaton Mountains, Arizona: implications for petrologic classification from thermal infrared remote sensing data. Journal of Geophysical Research, 109(E03007)

Misra, A. (2008) ASTER-based Lithologic and Alteration Mapping in Khetri Copper Belt, India, Unpublished PhD Thesis

MMAJ, (2001). Report on overseas satellite remote sensing survey program: Indochina malay project: Myanmar. 207p. (in Japanese with English appendix)

Ninomiya, Y.; Fu, B.; Cudahy, T.J. (2005) Detecting lithology with Advanced Spaceborne Thermal Emission and Reflection Radiometer (ASTER) multispectral thermal infrared "radiance-at-sensor" data. Remote Sensing of Environment, 99, pp. 127-139.

Prasad, D.N., Dotiwala, S.F., Agarwal, R.P., Mitra, D.S., and Bhoj, R., (1991). Interpretation of Airborne Synthetic Radar (SAR) Data for Structural and Lithological Detailing in Andaman, Islands. Unpublished ONGC Report.

Salisbury, J. W. and D'Aria, D. M., (1992). Emissivity of terrestrial materials in the 8-14 μm atmospheric window. Remote Sensing of Environment, 42, pp. 83-106.

van der Meer, F.D., van der Werff, H.M.A., van Ruitenbeek, F.J.A., Hecker, C.A., Bakker, W.H., Noomen, M.F., van der Meijde, M., Carranza, E.J.M., de Smeth, J.B., and Woldai, T. (2012). Multi- and hyperspectral geologic remote sensing: A review. International Journal of Applied Earth Observation and Geoinformation, vol. 14, pp.112-128.

Vaughan, R. G., Calvin, W. M. and Taranik, J. T. (2003). SEBASS Hyperspectral thermal infrared data: surface emissivity measurements and mineral mapping. Remote Sensing of Environment, 85, pp. 48-63.

Vaughan, R. G., Hook, S. J., Calvin, W. M. and Taranik, J. V., (2005). Surface mineral mapping at Steambot Springs, Nevada, USA, using multi-wavelength thermal infrared images. Remote Sensing of Environment, 99(1-2), pp. 140-158.

Watanabe,H., (2002). Rock type classification by multi-band TIR of ASTER. In: Annual General Meeting of the Geological Remote Sensing Group 'ASTER Unveiled', Burlington House, Piccadilly, London, UK.

Acknowledgements

The author(s) are grateful to Director (Exploration), ONGC for permission to share the results of work undertaken as part of R&D activities at KDMIPE, ONGC. Sincere thanks are due to Head KDMIPE, Head Geology Group, KDMIPE and Incharge Remote Sensing & Geomatics, KDMIPE for facilitation, encouragement and advice during the course of the studies. Support by colleagues at RS&G, KDMIPE, namely – Mr. D.K. Dangwal and Ms Prapti Semwal are gratefully acknowledged. The views expressed in the paper are solely of the author(s) and need not reflect those of the organization they represent.